Article

Light patterning semiconductor nanoparticles by modulating surface charges

Xiaoli He[1], Hongri Gu [2], Yanmei Ma[1], Yuhang Cai[1], Huaide Jiang[1], Yi Zhang[1], Hanhan Xie[1], Ming Yang[1], Xinjian Fan[3], Liang Guo[4], Zhan Yang [3] ✉ & Chengzhi Hu [1] ✉

Optical patterning of colloidal particles is a scalable and cost-effective approach for creating multiscale functional structures. Existing methods often use high-intensity light sources and customized optical setups, making them less feasible for large-scale microfabrication processes. Here, we report an optical patterning method for semiconductor nanoparticles by light-triggered modulation of their surface charge. Rather than using light as the primary energy source, this method utilizes UV-induced cleavage of surface ligands to modify surface charges, thereby facilitating the self-assembly of nanoparticles on a charged substrate via electrostatic interactions. By using citrate-treated ZnO nanoparticles, uniform ZnO patterns with variable thicknesses can be achieved. These multilayered ZnO patterns are fabricated into a UV detector with an on/off ratio exceeding 10^4. Our results demonstrate a simple yet effective way to pattern semiconductor nanoparticles, facilitating the large-scale integration of functional nanomaterials into emerging flexible and robotic microdevices.

The integration of colloidal nanoparticles into microdevices holds promise for many emerging technologies, such as smart dust[1,2], photoelectric devices[3], wearable electronics[4], miniature robots[5,6], and medical implants[7,8]. A critical step in their manufacture is the precise arrangement of these functional nanoparticles, which faces numerous challenges, including cost-effectiveness, the ability to scale up, and achieving consistent outcomes—challenges that are not commonly faced in smaller production volumes. Importantly, this patterning process must be compatible with existing microfabrication workflows, particularly photolithography and solution-based etching and deposition. Despite significant advances in colloidal assembly, current patterning methods often struggle to balance efficiency and throughput and typically require the introduction of customized setups in cleanroom environments. For example, template-based methods such as nanoimprinting require direct contact with the sample[9,10], posing a risk of damaging valuable molds and thereby reducing their

lifespan and increasing costs. Moreover, high-resolution techniques such as inkjet printing[11,12] and dip-pen nanolithography[13] achieve impressive results, but at the expense of production speed, making them impractical for large-scale, wafer-size mass production.

Direct light patterning has emerged as a dynamic and flexible technique that utilizes an external light source to intricately organize colloidal particles into complex patterns[14–16]. This technique leverages the unique properties of light, such as its ability to achieve high spatial and temporal precision, to perform noncontact manipulation, and to tune its wavelength and polarization[17]. These features make optical patterning particularly effective for tailoring the spatial arrangement and overall structure of colloidal nanoparticles. However, many light patterning techniques require very high light intensities because the driving mechanism is directly linked to the optical energy input to overcome fluidic drag. For example, optical tweezers use radiation pressure proportional to the light intensity and require a focused laser

[1]Shenzhen Key Laboratory of Biomimetic Robotics and Intelligent Systems, Department of Mechanical and Energy Engineering, Southern University of Science and Technology, Shenzhen, China. [2]Department of Physics, University of Konstanz, Konstanz, Germany. [3]School of Mechanical and Electrical Engineering, Soochow University, Suzhou, China. [4]SUSTech Energy Institute for Carbon Neutrality, Southern University of Science and Technology, Shenzhen, China. ✉e-mail: yangzhan@suda.edu.cn; hucz@sustech.edu.cn

(with a light intensity of 10^9–10^{11} mW cm^{-2}) to trap a colloidal particle[18,19]. In other examples, lasers are used to locally heat the medium to generate thermal gradients[20] or microbubbles[21,22] to trap colloidal particles. Currently, these methods rely heavily on lasers and intricate optical setups in laboratory environments, which is too early for wafer-scale high-throughput implementation in cleanrooms. Similar to dip-pen nanolithography and inkjet printing, enhancing the throughput of these optical patterning methods tends to prolong the duration of the process.
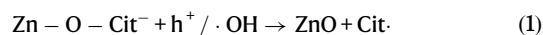
Reducing the need for high-intensity light in colloidal patterning can be achieved by rethinking light not as a primary energy source but as a carrier of patterning information. The goal is to align light power requirements with the capabilities of UV lamps (≈100 mW cm^{-2}), which are widely accessible in cleanrooms. A notable innovation that illustrates this concept is the development of optoelectronic tweezers, which use a localized electric field to significantly increase manipulation forces beyond the capabilities of optical tweezers[23,24]. In an optoelectronic system, the primary energy driving the assembly of particles comes from an alternating electric field, dramatically reducing the light intensity required by several orders of magnitude. Another direction is to harness the ambient thermal energy and the intrinsic chemical energies present in the colloidal system. This concept is echoed in the literature in the patterning of molecules and much smaller nanoparticles (<10 nm). Under UV irradiation, photoreactive surface ligands can bind directly to their neighboring nanoparticles, providing a convenient way to pattern using standard photolithography. Various inorganic materials, especially quantum dots, can be patterned using different surface chemical reactions[15,25]. Besides, various photosensitive ligands and additives have been investigated for the direct optical patterning of inorganic nanomaterials[26–28]. These investigations mainly focus on photochemical decomposition or transformation[15,29,30] (e.g., light exposure directly induces a solubility change in nanoparticle layers) and photoactive crosslinking of ligands (e.g., azide[25], benzophenone[26], and cinnamoyl compounds[31]). In these examples, the energy comes from the chemical potential of the surface ligand molecules, and light serves only as a trigger. Extending this principle to larger colloids that utilize ambient energy can expand the applications of large-scale colloidal patterning by eliminating the need for high-intensity light sources.

In this work, we develop a large-scale colloidal patterning method for semiconductor nanoparticles using light-triggered modulation of their surface charge. Upon exposure to UV light, ZnO nanoparticles are activated to absorb photons, initiating a reaction that cleaves the surface-bound citrate ligands. This process changes the surface charge of the original nanoparticles, allowing them to adhere to the negatively charged substrate by electrostatic attraction. In addition, this photochemical reaction releases Zn^{2+} ions and forms interparticle chemical bonds on adjacent nanoparticles, allowing the stacking of multilayer ZnO nanoparticle superstructures. By further modifying the surface ligands, we can adjust the surface charge, enabling both positive and negative patterning on the same substrate. Our method stands out for its simplicity and efficiency, requiring only a short exposure time (less than 2 min) and low optical intensity (as low as 6 mW cm^{-2}), making it a viable option for the mass production of semiconductor nanoparticle patterns at low cost. In addition, our patterning technique is compatible with various substrates, including transparent rigid glass and flexible polyvinyl chloride (PVC), laying the groundwork for future adaptation to flexible electronic devices. Moreover, we have extended this versatile approach to other semiconductor nanoparticles such as ZnS and TiO$_2$, demonstrating its broad applicability without the need for high-intensity light sources or complex equipment. To demonstrate the practical utility of our approach, we fabricate a photodetector from patterned ZnO colloidal arrays, which exhibits excellent optoelectronic properties characterized by a high on/off ratio up to 10^4.

Results

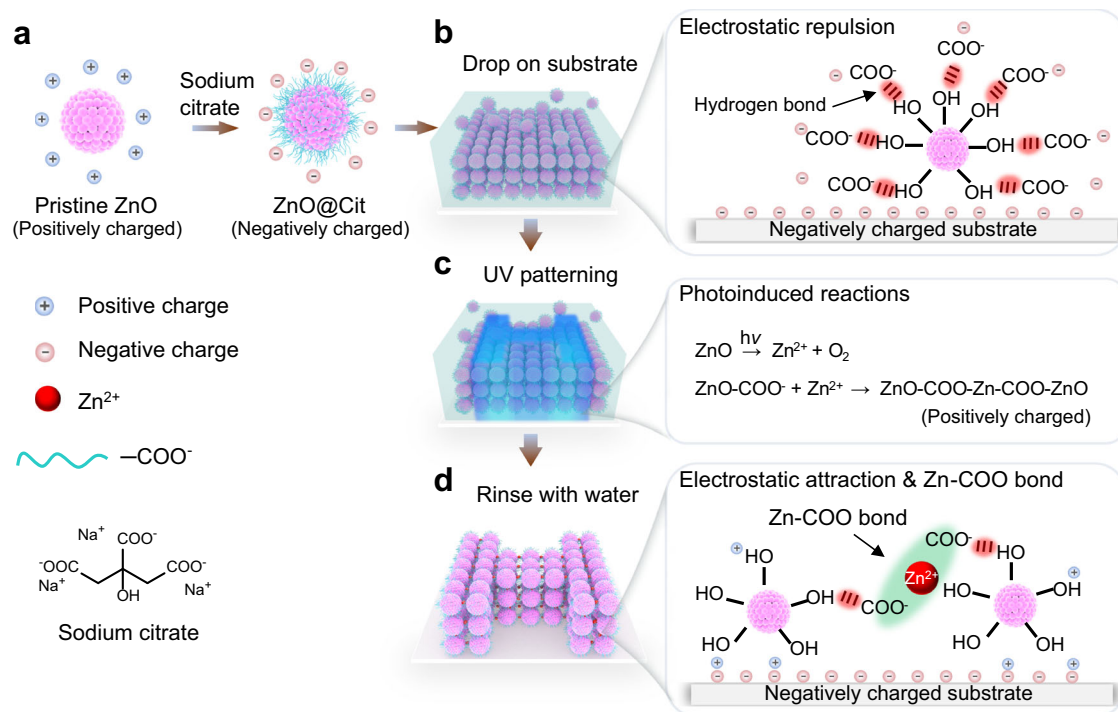### Positive patterning of ZnO@Cit nanoparticles

The elaborate modification of surface-capping ligands or functional groups to nanoparticles can regulate their surface charge, stability, or reactivity[28]. Semiconductors such as ZnO and TiO$_2$ can produce strong oxidative species such as superoxide radicals and hydroxyl radicals (·OH) under light irradiation[32]. In this context, surface ligands grafted onto semiconductor colloidal particles may undergo photodegradation, thereby altering their surface electrical properties. Such light-induced surface charge regulation can be used to enhance (positive patterning) or reduce (negative patterning) their adhesion to a charged substrate. Figure 1 illustrates the procedures for the positive patterning of ZnO nanoparticles via light-induced charge reversal and interparticle chemical bonding. Initially, pristine positively charged ZnO nanoparticles with abundant hydroxyl groups were surface-modified with sodium citrate, in which the citrate ligands were bound to the ZnO particles via hydrogen bonding[33]. The resulting citrate-capped ZnO nanoparticles (denoted as ZnO@Cit) acquired a negative charge due to the ionization of carboxyl groups (COO$^-$) from the citrate ligands. When an aqueous solution of these negatively charged ZnO@Cit nanoparticles was applied to a substrate with a negative surface charge, the electrostatic forces caused these particles to repel the substrate. Moreover, the surface charge of the nanoparticles was sufficiently repulsive to prevent random aggregation, enabling the particles to exhibit Brownian motion. Upon UV excitation, ZnO absorbs light energy and generates electrons and holes at its surface. The photogenerated holes (h$^+$) could react with H$_2$O molecules and produce ·OH and H$^+$. Both holes and ·OH have strong oxidation capabilities, leading to the decomposition of the citrate ligands on the ZnO surface and the production of carboxyl radicals (Cit·)[34]:

$$Zn - O - Cit^- + h^+ / \cdot OH \rightarrow ZnO + Cit\cdot \qquad (1)$$

where Cit = HO-CR$_2$-COO, and R = -CH$_2$COOH.

This transformation alters the surface charge of the original ZnO nanoparticles from negative to positive, enabling them to adhere to the negatively charged substrate via electrostatic attraction. Simultaneously, ZnO is prone to photocorrosion, releasing Zn^{2+} ions through the following reaction: ZnO + h$^+$ → Zn^{2+} + O$_2$[35]. Consequently, the released Zn^{2+} ions readily bond with COO$^-$ groups from adjacent ZnO@Cit nanoparticles via COO-Zn bonding. Due to the electrostatic attraction between the nanoparticles and the substrate, along with interparticle COO-Zn bonding, ZnO nanoparticles in the UV-irradiated region adhere to the substrate. In contrast, particles in the non-irradiated region can be easily removed by rinsing with deionized (DI) water, due to the electrostatic repulsion between the negatively charged particles and the substrate.

The diameter of the ZnO colloidal particles can be easily controlled within 250 to 700 nm by adjusting the amount of the seeding solution in a two-stage synthesis reaction (Suppl. Fig. 1)[36,37]. In this work, ZnO nanoparticles with a diameter of ≈600 nm were used as an example to illustrate the patterning method. The morphology of these ZnO nanoparticles was characterized using scanning electron microscopy (SEM) and transmission electron microscopy (TEM). As illustrated in Fig. 2a, the prepared pristine ZnO nanoparticles exhibited uniform sizes and spherical shapes. Each nanoparticle was composed of nanocrystals measuring 20-30 nm, resulting in a rough surface that offers abundant active sites for ligand grafting (Fig. 2b). These ZnO nanoparticles displayed a narrow size distribution (Fig. 2c). After surface modification with sodium citrate, ZnO@Cit nanoparticles grafted with carboxyl groups were obtained. The crystalline structures of both pristine ZnO and ZnO@Cit nanoparticles were examined using X-ray diffraction (XRD). As depicted in Fig. 2d, the XRD patterns of these two samples were congruent and closely matched the established JCPDS file (No. 36-1451) for ZnO with a hexagonal wurtzite crystal lattice. This

Fig. 1 | Scheme of the positive patterning of ZnO@Cit nanoparticles. a Pristine ZnO nanoparticles with a positively charged surface are modified with sodium citrate, introducing COO⁻ groups and forming ZnO@Cit (ZnO-COO⁻ in ionic form). **b** An aqueous dispersion of ZnO@Cit is applied to a negatively charged substrate, leading to electrostatic repulsion between the substrate and the ZnO@Cit nanoparticles. **c** UV irradiation induces the photodegradation of surface COO⁻ groups and initiates the release of Zn^{2+} ions through photocorrosion, thereby altering the surface potential of ZnO nanoparticles from negative to positive. **d** This dynamic process triggers the formation of interparticle Zn-COO bonds, allowing for multi-layered deposition of ZnO@Cit nanoparticles onto a negatively charged substrate via electrostatic attraction.

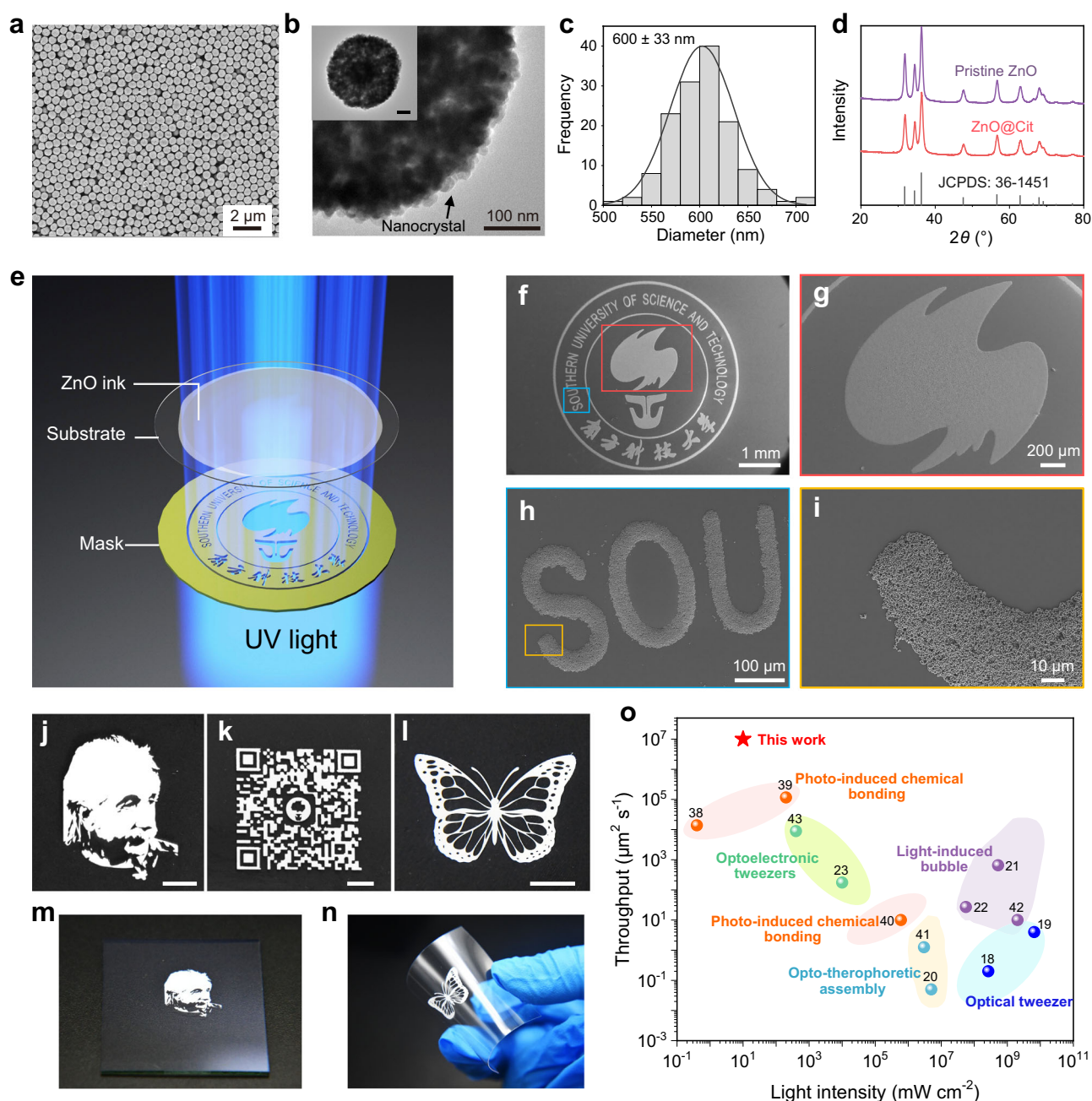confirms that citrate modification had no discernible impact on the crystal structure of ZnO.

To demonstrate the capability of UV-induced patterning of ZnO@Cit nanoparticles, we fabricated several patterns on various transparent substrates employing a custom-made optical patterning system, as shown in Fig. 2e. UV light was emitted from a xenon lamp placed below the photomask, creating a light pattern on the ZnO@Cit suspension dripped onto the transparent substrate. Different UV illumination intensities can be obtained by adjusting the distance between the lamp and the sample (Suppl. Fig. 2). As shown in Fig. 2f, the ZnO@Cit nanoparticle pattern of the SUSTech logo was deposited on a glass substrate after UV illumination at 6 mW cm⁻² for 10 s, with the corresponding photomask patterns displayed in Suppl. Fig. 3. The enlarged SEM images in Fig. 2g–i clearly show that the nanoparticles in the UV-irradiated region remained, while those in the nonirradiated region were removed during the water-rinsing process. Additional intricate patterns of ZnO@Cit nanoparticles printed on glass substrates are shown in Fig. 2j–l, demonstrating precise replication of photomask patterns and consistent, reliable optical patterning of different layouts. To produce patterns larger than the UV spot size, we scanned the ZnO@Cit nanoparticles back and forth using a fiber optic probe at a speed of 10 cm s⁻¹. As shown in Suppl. Fig. 4, a butterfly pattern with dimensions of 2 cm in width and 3 cm in length was achieved within 1 min. Apart from depositing ZnO nanoparticles on standard nonconductive glass substrates, we conducted optical patterning on conductive ITO glass substrates (Fig. 2m). Our room temperature patterning process allows ZnO nanoparticles to be patterned on flexible substrates that are not resistant to high temperatures. As shown in Fig. 2n, a butterfly was created on a PVC substrate. The ability to photopattern semiconductor nanoparticles on both conductive and flexible substrates provides opportunities for the use of ZnO-based flexible electronics in various applications.

We compared our method to other solution-based light patterning techniques for colloidal nanoparticles in terms of throughput and required light exposure (Fig. 2o and Suppl. Table 1)[18–23,38–43]. Our work requires an optical intensity of 6 mW cm⁻² to generate a centimeter-scale pattern in 10 s. The required exposure dose is at least four orders of magnitude lower than that of most laser-based patterning methods[18–23,40–42]. Besides, our method exhibits scalability to achieve intricate centimeter-scale patterns with a microscale resolution of ≈20 μm (Suppl. Fig. 5).

The positive patterning of ZnO@Cit particles on a substrate involves two key processes: electrostatic attraction between the nanoparticles and the substrate, and chemical bonding between nanoparticles. UV irradiation induces the photodegradation of citrate ligands on the ZnO surface and the photocorrosion of ZnO, leading to a change in the surface charge of the nanoparticles. As shown in Fig. 3a, carboxyl-functionalized ZnO@Cit nanoparticles initially dispersed in pure water exhibited a negative zeta potential of −18.5 mV. However, after short UV irradiation (6 mW cm⁻²) of 15 s, this value increased to +40 mV. For comparison, ZnO@Cit particles maintained a negative surface charge when dispersed in a low-concentration citrate solution (0.1 mM). Despite the UV-induced photochemical degradation of citrate ligands on the ZnO surface, the free citrate ligands in solution quickly interacted with the ZnO surface through hydrogen bonding and electrostatic attraction, maintaining the negative charge of the ZnO@Cit nanoparticles. It is worth mentioning that ZnO@Cit nanoparticles, when dispersed in a high-concentration citrate solution (such as 0.1 M), tend to adhere to the substrate due to the quenching of the electric double layers. Since the surface of a glass substrate is typically negatively charged when it is in contact with aqueous solutions[44], positive patterning of ZnO@Cit particles can be achieved.

To validate the significance of electrostatic attraction, we first investigated the changes in the motion state of ZnO@Cit particles in
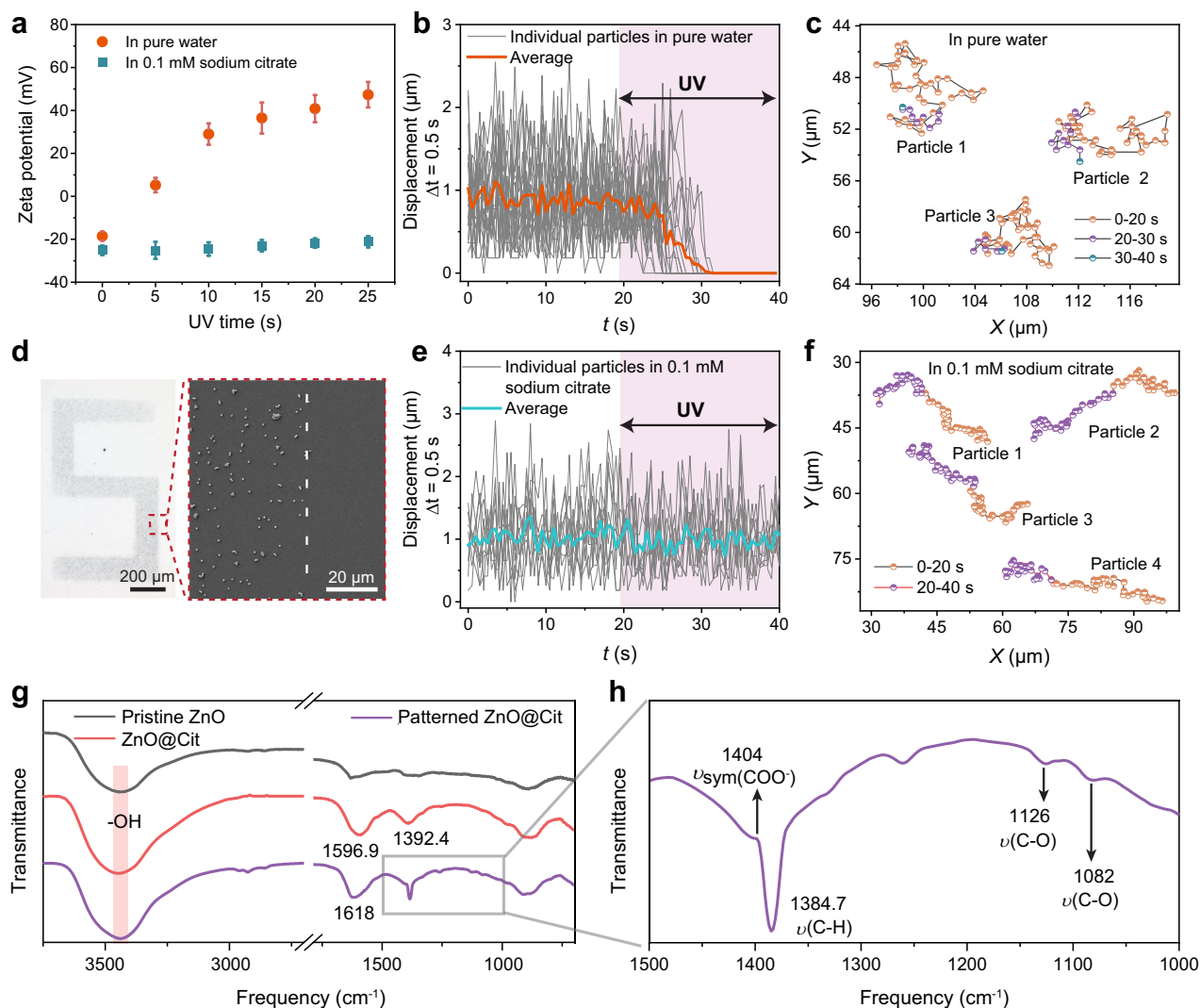
Fig. 2 | Material characterization and positive patterning of ZnO@Cit nanoparticles. a SEM image and **b** TEM image of pristine ZnO nanoparticles. Scale bar in the inset (**b**): 100 nm. **c** Size distribution of the ZnO nanoparticles. **d** XRD patterns of both the pristine ZnO and ZnO@Cit samples. **e** Schematic diagram of the experimental setup used for photopatterning of ZnO nanoparticles. **f**–**i** SEM images showcasing the patterned SUSTech logo. **g** Enlarged area highlighted in red in (**f**). **h** Enlarged area highlighted in bright blue in (**f**). **i** Enlarged area highlighted in golden yellow in (**h**). Photographs of a patterned portrait of Albert Einstein. **j** A QR code redirecting to the official WeChat account of SUSTech (**k**), and a butterfly (**l**) on glass substrates. Scar bars: 2 mm in (**j**) and (**k**), 5 mm in (**l**). **m** Photopatterning on ITO glass (4 × 5 cm²). **n** Photopatterning on flexible PVC substrates. **o** Comparison of our work with reported light-induced patterning methods. The throughput is the ratio of the patterned area (μm²) to the required irradiation time (s), or the product of the scan rate (μm s⁻¹) and the width of the printed line (μm). The SUSTech logo has been reproduced with permission from Southern University of Science and Technology. The image of Albert Einstein in (**j, m**) is adapted with permission from Philippe Halsman Archive (©Philippe Halsman/Magnum Photos/IC photo). The butterfly image is adapted with permission from openclipart.org (https://openclipart.org/detail/228436/butterfly-1-black, CC0 1.0). Source data are provided as a Source Data file.

pure water before and after exposure to UV light. In the experiment, a low concentration of ZnO nanoparticles (0.1 mg mL⁻¹) was used to ensure considerable separation between nanoparticles to eliminate the potential effects of chemical bonding arising from Zn²⁺ in photochemical reactions. Figure 3b, c shows the displacements of individual ZnO@Cit nanoparticles (*N* = 20) at 0.5 s intervals in pure water, along with their typical motion trajectories (Suppl. Movie 1). In the absence

of light irradiation, ZnO@Cit nanoparticles exhibited random motion in pure water. However, upon exposure to low-intensity UV light (6 mW cm⁻²) for 10 s, they adhered directly to the substrate. Besides, there was no observed particle aggregation but rather the direct deposition of particles on the substrate. Subsequently, a monolayer of ZnO@Cit particles was deposited on the substrate after rinsing (Suppl. Fig. 6a), enabling the creation of a monolayered pattern (Fig. 3d)
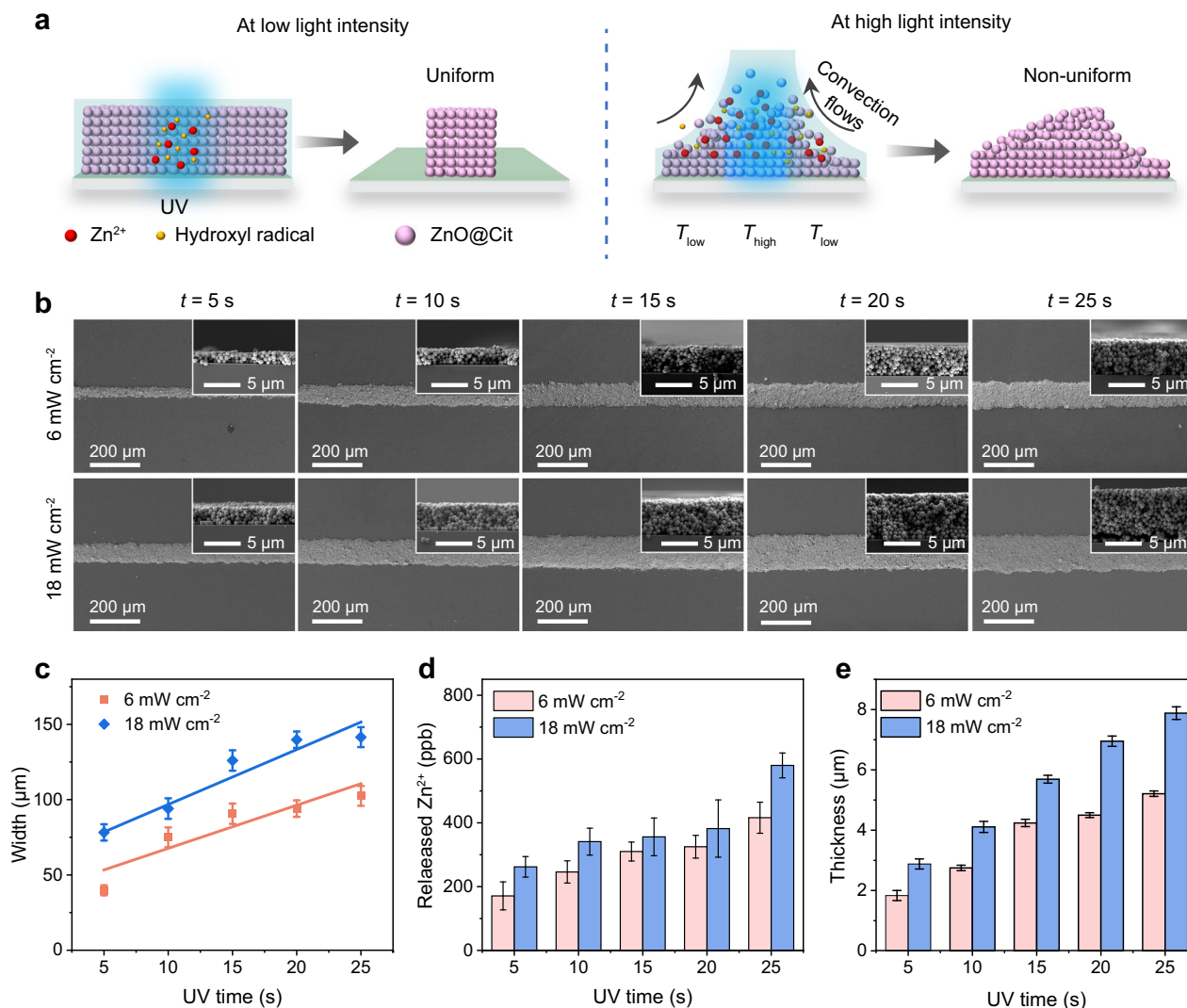
Fig. 3 | Verification of positive patterning mechanism. a Zeta potential plots of ZnO@Cit particles dispersed in pure water and 0.1 mM sodium citrate aqueous solution versus exposure time. Data were presented as the mean values ± SD, $n = 3$ independent measurements. Motion behaviors of ZnO@Cit particles (**b**, **c**) in pure water and (**e**, **f**) in 0.1 mM sodium citrate solution before and after UV exposure. **d** Optical image (left) and SEM image (right) of the monolayered "S" shape obtained by patterning ZnO@Cit particles at a low concentration (0.1 mg mL⁻¹). **g** FTIR spectra of pristine ZnO, ZnO@Cit, and patterned ZnO@Cit nanoparticles. **h** Enlarged FTIR spectrum of the patterned ZnO@Cit sample at 1500–1000 cm⁻¹. Source data are provided as a Source Data file.

through electrostatic attraction. In contrast, ZnO@Cit nanoparticles dispersed in a 0.1 mM sodium citrate aqueous solution maintained a negative surface charge after UV illumination (Fig. 3a). In this scenario, both the substrate and particles were negatively charged, so the particles sustained their Brownian motion after UV exposure (Fig. 3e, f), unlike those in pure water. Consequently, almost all the particles were washed away from the glass substrate during the rinsing process (Suppl. Fig. 6b), demonstrating that the light-induced reversal of the particle surface charge is essential for achieving optical patterning on a negatively charged substrate.

When a high concentration of ZnO@Cit nanoparticles is used, photochemically released Zn^{2+} ions can coordinate with COO^- groups from adjacent ZnO@Cit nanoparticles, forming interparticle Zn-COO bonds[45,46]. This coordination initiates the multilayered patterning of ZnO@Cit nanoparticles on the substrate. We conducted Fourier transform infrared (FTIR) spectroscopy on pristine ZnO, ZnO@Cit, and patterned ZnO@Cit samples. As depicted in Fig. 3g, the unmodified ZnO spectrum manifests a distinct characteristic peak at 3442 cm⁻¹, indicating abundant hydroxyl groups on its surface[47]. These hydroxyl groups potentially serve as binding sites for COO^- groups through hydrogen bonding[33]. In the case of ZnO@Cit, the presence of grafted COO^- groups on the surface is confirmed by the appearance of distinctive peaks at 1597 and 1392 cm⁻¹, corresponding to the symmetric and asymmetric stretching vibrations of COO^- groups, respectively[48]. Upon UV exposure, discernible shifts in the FTIR peaks are observed in the pattern of ZnO@Cit. Specifically, the symmetric and asymmetric stretching modes of COO^- groups shift to 1618 and 1404 cm⁻¹, respectively. This light-induced shift can be attributed to the chemical interaction between Zn^{2+} ions and COO^- groups. The significant difference of 214 cm⁻¹ between the asymmetric and symmetric stretching frequencies of COO^- in patterned ZnO@Cit indicates the coordination of carboxyl groups with Zn^{2+} ions through an unidentate mode[49]. Furthermore, several new peaks appear in the spectrum of the UV-exposed ZnO@Cit sample (Fig. 3h). The sharp peak at 1384.7 cm⁻¹ is ascribed to the vibration of C-H, while the peaks at 1126 and 1082 cm⁻¹ can be attributed to the stretching vibration of C-O and the stretching vibration of C-C of zinc acetate, respectively, providing evidence for the formation of Zn-COO bonds[50,51]. Thus, the positive patterning of ZnO nanoparticles mainly involves photoinduced surface potential reversal resulting from the partial cleavage of the citrate ligand and the formation of Zn-COO chemical bonds between nanoparticles due to the release of Zn^{2+}. Following a similar procedure, ZnO@Cit

Fig. 4 | Influence of light intensity and exposure time on positive patterning.
a Schematic diagram of the influence of light intensity on ZnO@Cit patterns.
b Top-view and cross-sectional-view (inset) SEM images of lines printed at different exposure times and light intensities with a line-shaped (40 μm in width) photomask. **c** Relationship between the width of the printed line pattern and the UV irradiation time under different UV light intensities (Error bar represents $n = 5$

independent measurements). **d** Amount of released Zn^{2+} under different UV irradiation conditions (Error bar represents $n = 3$ independent samples).
e Relationship between the thickness of the printed line pattern and the UV irradiation time under different UV light intensities (Error bar represents $n = 5$ independent measurements). Source data are provided as a Source Data file.

microspheres (2–4 μm) and ZnO@Cit nanoparticles with irregular shapes were also photopatterned (Suppl. Fig. 7).

In addition to citrate ligands, our photopatterning method can be implemented to ZnO nanoparticles capped with other surface ligands comprising carboxyl groups (Suppl. Fig. 8), such as 3-mercaptopropionic acid (MPA), malate, and tartrate. Besides, we have also achieved positive patterning of other semiconductor particles prone to photocorrosion, such as MPA-capped CdS (CdS@MPA) nanoparticles (Suppl. Fig. 9) and MPA-capped ZnS (ZnS@MPA) microparticles (Suppl. Fig. 10). Our method eliminates the need for conventional photoresists and enables the rapid patterning of multilayered colloidal semiconductor nanomaterials on various transparent substrates on a large scale.

Influence of light irradiation on positive patterning
As an optical patterning approach, both light intensity and illumination duration control the photopatterning quality (Suppl. Fig. 11). Under moderate irradiation doses and exposure times, photoinitiated reactive species such as ·OH and Zn^{2+} ions are generated only in the

exposed regions, facilitating the localized deposition of nanoparticles. This ensures that the patterned layer closely adheres to the photomask design, exhibiting uniformity and high fidelity. In contrast, when subjected to high-intensity UV illumination, heat generation on the semiconductor nanoparticles due to photothermal conversion becomes pronounced. While the heating effect due to UV photoabsorption by water is negligible, the strong UV absorption by ZnO nanoparticles under high-intensity UV illumination can trigger natural or Marangoni convection, lead to nonuniform pattern formation (Fig. 4a). As shown in Suppl. Fig. 12 and Suppl. Note 1, under high-intensity UV light (24 mW cm^{-2}), the temperature difference between the irradiated and nonirradiated area after 15 s was 1.5 °C, sufficient to induce natural convection[52,53]. Supplementary Fig. 13 further illustrates the difference between ZnO patterns formed under weak (6 mW cm^{-2}) and intense (24 mW cm^{-2}) UV irradiation. The ZnO thin film patterned at 6 mW cm^{-2} is flat and exhibits uniform thickness, while the ZnO film obtained at 24 mW cm^{-2} shows significant clustering and uneven thickness. Therefore, minimizing convection fluid flow caused by photothermal effects is essential to achieving consistent and high-quality patterns.

We investigated the influence of UV exposure duration on the width and thickness of line-shaped patterns at light intensities of 6 and 18 mW cm^{-2}, where no significant convection flow was observed throughout the experiment. Figure 4b presents the top-view and corresponding cross-sectional (inset) SEM images of ZnO@Cit line-shaped patterns obtained under different UV light intensities and illumination durations, using a line-shaped photomask with a width of 40 μm. The nanoparticles exhibited random packing with an estimated porosity of ≈66.82% (Suppl. Table 2 and Suppl. Fig. 14). At 6 mW cm^{-2} for 5 s, the obtained linewidth was 39.7 ± 3.2 μm, closely matching the designed width. Additionally, line widths of 40.5 ± 2.7 μm and 42.6 ± 3.1 μm were achieved at 3 mW cm^{-2} for 15 s and 12 mW cm^{-2} for 4 s, respectively (Suppl. Fig. 15). No discernible pattern was observed when the UV exposure time was less than 5 s at the low light intensity of 6 mW cm^{-2}. This is because the ZnO@Cit particles still remain strongly negatively charged due to the limited photodegradation of carboxyl groups, and the amount of Zn^{2+} ions is insufficient to form an adequate amount of Zn-COO bonding. At a given light intensity, increasing the UV exposure time resulted in a broader linewidth, which followed a linear trend as shown in Fig. 4c. The rate of increase in width was greater at higher light intensities. Specifically, at intensities of 6 and 18 mW cm^{-2}, the width increased at rates of 2.86 and 3.65 μm s^{-1}, respectively. The broadening effect can be attributed to light scattering inside the colloidal solution, the nondirectional nature of the xenon-lamp light (Suppl. Fig. 16), as well as ion diffusion from high concentration (irradiated) to low concentration (nonirradiated) regions. At the high UV light intensity of 24 mW cm^{-2}, the rate of width increase dramatically rose to 18.02 μm s^{-1}, resulting in a significant decrease in width resolution (Suppl. Fig. 17).

The generation of Zn^{2+} and subsequent formation of Zn-COO bonds account for the multilayered optical patterning. The amount of released Zn^{2+} ions under different UV irradiation conditions was detected by inductively coupled plasma-mass spectrometry (ICP-MS) and was found to be directly proportional to both the exposure time and light intensity (Fig. 4d). Cross-sectional SEM images of the line patterns, shown in the insets of Fig. 4b, reveal the formation of multiple layers, with thicknesses ranging from 1.7 to 8 μm. As illustrated in Fig. 4e, the thickness of the patterned ZnO@Cit layers increased steadily under UV exposure at both low (6 mW cm^{-2}) and medium (18 mW cm^{-2}) light intensities. However, intense UV irradiation (24 mW cm^{-2}) can induce thermal convection flow, leading to the upward movement of ZnO@Cit particles within the UV-illuminated region. Such upward motion disrupted the formation of Zn-COO bonds, resulting in a thinner layer with an uneven and unpredictable thickness (Suppl. Fig. 17). Applying light in a pulsed manner or implementing cooling techniques could help to minimize the thermal effects, thereby facilitating pattern formation (see Suppl. Note 2 and Suppl. Fig. 18).

Negative patterning of ZnO@Cit/PDDA particles

The proposed light-induced alteration in zeta potential can also be applied to the negative patterning of colloidal particles. In this circumstance, nanoparticles in the illuminated area are washed away due to a reduction in electrostatic forces, while those in the nonilluminated region remain attached. As illustrated in Fig. 5a, the negatively charged ZnO@Cit nanoparticles were further capped with poly(diallyl dimethyl ammonium chloride) (PDDA), which contains abundant positively charged ammonium groups, resulting in ZnO@Cit/PDDA nanoparticles acquiring a positive charge. The attachment of the PDDA layer to the ZnO@Cit surface was confirmed by TEM. As shown in Suppl. Fig. 19, the N and Cl signals from PDDA were clearly observed, along with the Zn and O signals from ZnO@Cit, suggesting the successful coating of ZnO@Cit with PDDA. Upon applying the ZnO@Cit/PDDA aqueous dispersion onto a negatively charged substrate, the nanoparticles on the bottom adhered tightly to the substrate due to the strong electrostatic attractive force, forming a monolayer of
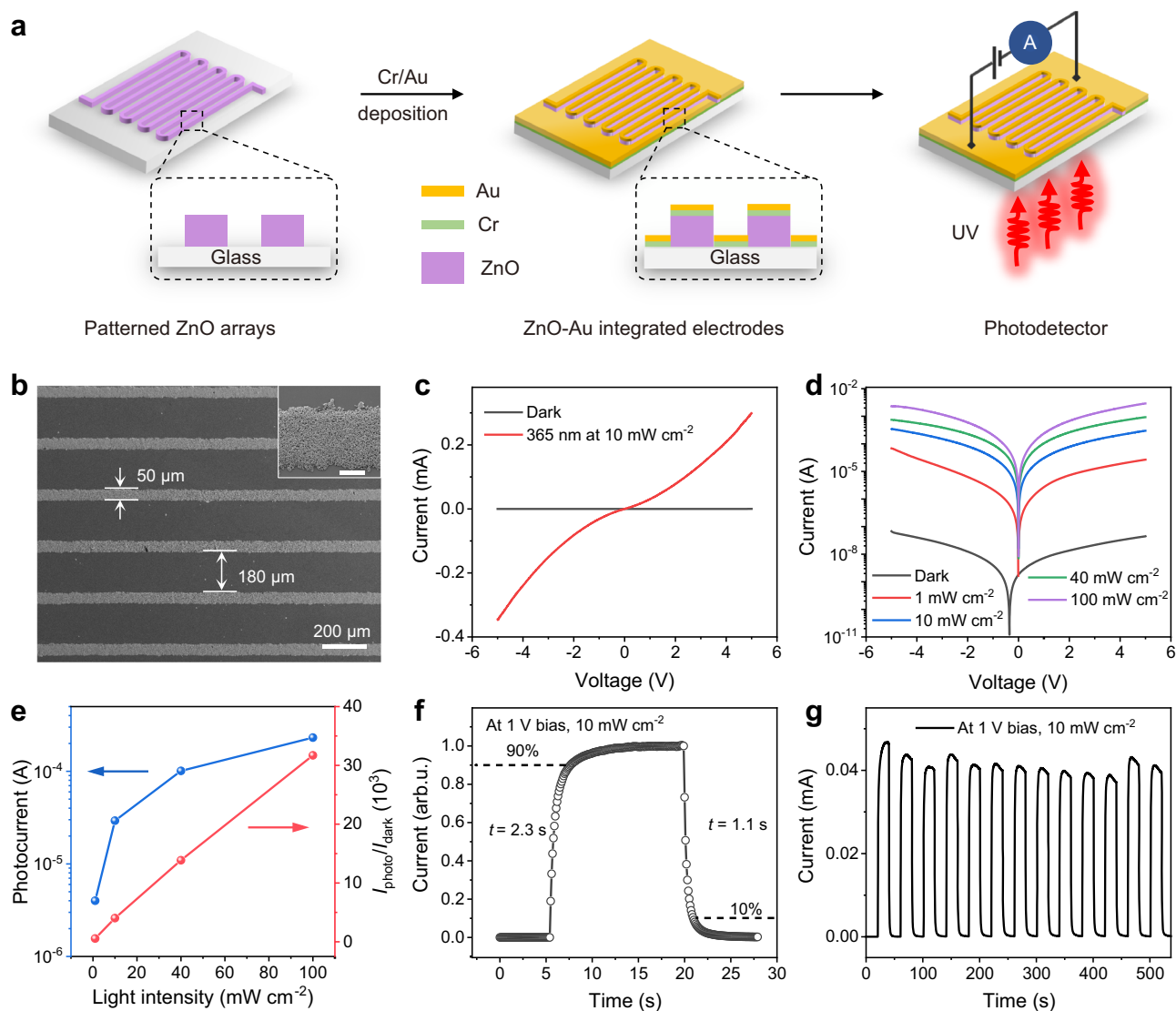
nanoparticles with a coverage rate of 45.2% after rinsing with water (Suppl. Fig. 20). Under UV irradiation, highly reactive holes and ·OH were generated at the ZnO-water interface. These radicals partially photodegraded the attached citrate and PDDA ligands, reducing the positive charges on the ZnO surface and weakening the electrostatic force between the nanoparticles and the substrate. Consequently, nanoparticles in the UV-exposed region were removed upon rinsing, facilitating the negative patterning of ZnO nanoparticles.

As shown in Fig. 5b, the zeta potential of ZnO@Cit/PDDA was initially +44 mV and decreased to +12 mV after 80 s of UV illumination. This decrease in zeta potential was caused by the partial decomposition of the surface ligands under UV irradiation, as further confirmed by X-ray photoelectron spectroscopy (XPS). High-resolution XPS spectra in the C 1s and N 1s regions revealed significant changes after irradiation (Fig. 5c–e). Specifically, the relative content of the C-O/C-N peak at 286.34 eV decreased from 27.35 to 16.15% after UV irradiation. Additionally, the detachment of PDDA molecules led to a substantial reduction in the N 1s peak intensity (Fig. 5c), with the atomic content of N decreasing from 3.07 to 0.78% (Suppl. Table 3). These results, from both zeta potential and XPS analysis, conclusively demonstrate that UV irradiation induces the cleavage of citrate and PDDA ligands on the ZnO surface.

Figure 5f–i presents the negative patterning of ZnO@Cit/PDDA on a glass substrate, depicting the SUSTech logo. This patterning was achieved using the same experimental setup as described in Fig. 2e. The white areas shown in Fig. 5f represent ZnO nanoparticles, while the dark areas indicate the bare substrate. Upon examining the magnified SEM images in Fig. 5g–i, almost all particles in the illuminated area were washed away, leaving a uniform thin layer in the unexposed area. Additionally, Fig. 5j–l shows various other patterns formed using ZnO@Cit/PDDA, including a QR code and a butterfly on a glass substrate, as well as a butterfly pattern on a flexible PVC substrate. The negative pattern resolution by ZnO@Cit/PDDA is ≈16 μm, as indicated in Suppl. Fig. 21. Similar to positive patterning, the negative printed linewidth increases with exposure time (Fig. 5m), while maintaining a particle removal efficiency of ≈98% (Suppl. Fig. 22). This increase is due to the diffusion of photo-generated carriers and radicals to the nonilluminated region, inducing the cleavage of surface ligands in neighboring unexposed regions. Consequently, excessively prolonged exposure times for a specific pattern can lead to distortion of the negative pattern, as demonstrated in Suppl. Fig. 23. These successful negative patterns using ZnO@Cit/PDDA nanoparticles confirm the feasibility and versatility of patterning semiconductor colloidal particles through light-mediated zeta potential changes. Other semiconductor particles with PDDA ligands can also be optically patterned similarly. For example, we synthesized pristine TiO$_2$ microparticles (diameter: 1.1 μm) with a negative surface charge (zeta potential: −22 mV) and functionalized them with a PDDA layer to obtain TiO$_2$/PDDA (zeta potential: +34 mV). As shown in Suppl. Fig. 24, due to the large surface charge, TiO$_2$/PDDA microparticles were deposited onto the negatively charged substrate via electrostatic assembly. TiO$_2$ shares a similar energy band structure with ZnO and can generate electron-hole pairs with strong redox reactivity upon UV excitation, leading to the photodecomposition of the surface PDDA layer. Therefore, the zeta potential of TiO$_2$/PDDA decreased with exposure time (Suppl. Fig. 25), weakening the electrostatic attraction between the particles and the substrate. After 100 s of irradiation at 6 mW cm^{-2}, clear TiO$_2$/PDDA patterns were obtained (Suppl. Fig. 26). Their linewidth also increased linearly with exposure time (Suppl. Fig. 27). Under the same light intensity, TiO$_2$/PDDA typically required a longer exposure time (over 80 s) compared to ZnO@Cit/PDDA (≈10 s) to achieve a negative pattern. We attribute this to the higher photostability of TiO$_2$ than that of ZnO[54]. Photocorrosion in ZnO can accelerate the detachment of surface ligands, resulting in a faster patterning

Fig. 5 | Negative patterning of ZnO@Cit/PDDA particles. a Schematic diagram of the negative patterning process. **b** Zeta potential of ZnO@Cit/PDDA particles after UV irradiation at 6 mW cm^{-2}. (Error bar represents $n = 3$ independent measurements). **c** XPS N1s spectra of ZnO@Cit/PDDA particles before and after UV irradiation. **d**, **e** XPS C1s spectra of ZnO@Cit/PDDA particles before and after UV irradiation, respectively. **f** Digital image of negatively patterned SUSTech logo with ZnO@Cit/PDDA **g**, **h** SEM images of the enlarged areas highlighted in red and bright blue in (**f**), respectively. **i** SEM image of the enlarged area highlighted in blue in (**h**).

Digital photos of printed QR code of the official WeChat account of SUSTech (**j**) and butterfly (**k**) on glass substrates and butterfly (**l**) on flexible PVC substrates. Scar bar in (**j**): 2 mm. Scar bar in (**k**): 5 mm. **m** Relationship between the width of the printed line pattern for ZnO@Cit/PDDA and the exposure time (Error bar represents $n = 5$ independent measurements). The SUSTech logo has been reproduced with permission from Southern University of Science and Technology. The butterfly image is adapted with permission from openclipart.org (https://openclipart.org/detail/228436/butterfly-1-black, CC0 1.0). Source data are provided as a Source Data file.

process. In addition, distortion of the pattern was also observed in TiO₂/PDDA when the exposure time was longer than 160 s (Suppl. Fig. 28). Beyond ZnO and TiO₂, we also achieved negative photo-patterning of ZnS microparticles (Suppl. Fig. 29) and CdS nanoparticles (Suppl. Fig. 30).

Demonstration of optically patterned ZnO in photodetectors

The light-induced patterning of ZnO colloidal nanoparticles, combined with a metal deposition process, can be used for the

construction of ZnO-based optoelectronic devices. As a proof-of-concept, we fabricated a UV-responsive ZnO photodetector. Figure 6a illustrates the fabrication process. ZnO arrays, with a linewidth of 50 μm and a spacing of 180 μm (Fig. 6b and Suppl. Fig. 31), were printed onto a glass substrate using ZnO@Cit nanoparticles, followed by electron beam evaporation of a 5 nm Cr layer and a 60 nm Au layer. Since the thickness of the ZnO layer (≈4 μm) is much greater than that of the conductive layer (65 nm), naturally formed Au interdigital electrodes with a width of 180 μm were obtained after the Au

Fig. 6 | Photodetector made of patterned ZnO nanoparticles. a Fabrication process of a metal-semiconductor-metal photodetector via optical patterning of ZnO arrays on a glass substrate coupled with a metal deposition technique. **b** SEM image of patterned ZnO arrays. Scale bar inset, 20 µm. **c** *I-V* curves of the ZnO photodetector in the dark and under 365 nm light illumination at 10 mW cm⁻². **d** Logarithmic *I-V* curves of the device under light illumination with different light intensities. **e** Photocurrent and photo-to-dark current ratios were measured at different light intensities with a 1 V bias. **f** Time response of the device at a 1 V bias. **g** *I-t* curve of the device at a 1 V bias upon switching the light illumination on/off. Source data are provided as a Source Data file.

deposition on the printed ZnO arrays, with ZnO serving as the active layer. The *I-V* curves and logarithmic *I-V* curves of the ZnO photodetector under different UV illumination conditions are depicted in Fig. 6c, d, respectively. The nonlinear current-voltage behavior implies the presence of Schottky contacts between ZnO and the Au electrodes. Figure 6e illustrates the photocurrent ($I_{photo} = I_{light} - I_{dark}$) measured at various light intensities with a 1 V bias, accompanied by the respective photo-to-dark current ratio (I_{photo}/I_{dark}). At a forward bias of 1 V, the dark current is ≈7.2 nA. Under an illumination intensity of 100 mW cm⁻², a much larger photocurrent of 231 µA is observed, yielding a high photo-to-dark current ratio of 3.2×10^4. Even under weak illumination of 1 mW cm⁻², this value reaches 541, indicating the excellent sensitivity of the designed photodetector. Figure 6f shows the transient photoresponse curve of the device. The rise time (t_r) and decay time (t_d) are defined as the duration of time during which the current increases to 90% of the steady state and decreases from 100 to 10%, respectively. The rise time and decay time were 2.3 and 1.1 s, respectively, indicating rapid chemo-physisorption and photo-desorption of oxygen molecules from the ZnO surface. The stability test was conducted under a bias of 1 V under chopped UV illumination at 10 mW cm⁻². As depicted in Fig. 6g, the current response to light irradiation fluctuates periodically, and the photocurrent remains steady at ≈40 µA after several on/off switches, demonstrating the reliability and reproducibility of the photodetector. Our ZnO photodetectors exhibit performance comparable to those reported in the literature (Suppl. Table 4, Suppl. Note 3, and Suppl. Fig. 32).

It is generally accepted that the UV detection mechanism of ZnO-based photodetectors can be attributed to the adsorption and desorption of O_2 molecules on the surface of ZnO colloidal particles[55,56]. In dark conditions, O_2 molecules adsorb onto the surface of ZnO particles and capture free electrons from the semiconductor, resulting in the formation of O_2^- ions, as described by the reaction: $O_2 + e^- \rightarrow O_2^-$. This process creates a depletion layer near the surface, characterized by low conductivity. Upon exposure to UV illumination, photogenerated holes migrate to the surface of ZnO particles, where they recombine with the adsorbed O_2^- ions, releasing the captured electrons back into the ZnO particles. This recombination increases the conductivity of the material. The high photoconductive gain observed in the designed

ZnO photodetector can be ascribed to both the large surface area and the grating structure[57]. As shown in Fig. 2b, each ZnO colloidal particle is composed of nanocrystals (10–20 nm), and many intercluster pores exist on the patterned ZnO film, providing a large internal surface as adsorption sites for O_2 molecules[37]. In addition, compared with planar film structure, the grating structure of ZnO enables higher carrier mobility due to a one-directional current path[57].

Discussion

The essence of our proposed method relies on the light-induced photochemical degradation of ligands on photocatalytic semiconductor nanoparticles, which allows for a substantial change of the nanoparticle surface charge, creating an overall charge that could promote or weaken their electrostatic interaction with charged substrates. Thus, extensive semiconductor nanoparticles can be potentially patterned by the proposed method. A successful practice relies on (1) coating of semiconductor nanoparticles with ligands that generate sufficiently strong surface charge; (2) photodegradation of the ligand when light irradiation with appropriate energy ($h\nu > E_g$) is exposed to the nanoparticle, which significantly reduces or reverses the surface charge of the nanoparticles. Further, for positive patterning semiconductor particles with multiple layers, their surface charge reversal and formation of metal-COO bonds are required under light irradiation. This requires the dissociation of partial carboxylate ligands, accompanied by the release of metal ions. The establishment of an effective and stable ligand coating is of great importance[28]. Citrate, MPA, malate, and tartrate have been proven feasible for capping ZnO nanoparticles. In contrast, we also found that other carboxyl-containing ligands, such as ethylenediaminetetraacetic acid disodium salt and glycine, can cause particle aggregation, thus inappropriate for positive optical patterning of ZnO nanoparticles.

We also investigated the positive patterning of ZnO@Cit nanoparticles on neutral and positively charged substrates (Suppl. Fig. 33). The neutral substrates were created by modifying glass slides with octadecyltrichlorosilane[58]. Due to the weak interaction between the particles and the neutral substrate, the ZnO@Cit particles were easily washed away by water, and no pattern was obtained. The positively charged substrates can be obtained by functionalizing with 3-aminopropyltriethoxysilane (APTES). ZnO@Cit nanoparticles can be patterned either positively or negatively for positively charged substrates, depending on the rinsing strength. After UV irradiation, when we gently rinsed the substrate, a positive pattern appeared (Suppl. Fig. 33b). In the nonirradiated regions, nanoparticles adjacent to the substrate were electrostatically attracted to the substrate, forming a monolayer film (Suppl. Fig. 33d). In contrast, in the irradiated regions, the release of Zn^{2+} ions facilitated the formation of Zn-COO bonds between adjacent ZnO nanoparticles, leading to the assembly of multilayered ZnO nanoparticle superstructures (Suppl. Fig. 33e). Although light irradiation weakened the electrostatic attraction between the nanoparticles and the substrate due to the photodegradation of citrate ligands, the multilayered particles remained intact after gentle rising. When we rinsed the substrate further, a negative pattern was obtained (Suppl. Fig. 33f). In this case, most nanoparticles in the illuminated area were washed away, while the nonilluminated areas retained a single layer of ZnO.

Since UV-induced citrate degradation and the formation of interparticle Zn-COO bonding are two competitive processes, the duration of citrate treatment significantly impacts the quality of the printed patterns. Suppl. Fig. 34 compares the printed ZnO films with different durations of citrate treatment. The result shows that only a single layer was obtained with short citrate treatment (4 h), whereas a thicker film (≈18 μm) was obtained when the citrate modification was extended to 60 h. With short citrate treatment, the content of the carboxyl group on the ZnO surface is insufficient, and most carboxyl groups undergo photodegradation, resulting in only a small portion

participating in the formation of interparticle chemical bonds. This makes it challenging to achieve a continuous multilayered pattern. Conversely, sufficiently long citrate treatment provides an adequate amount of carboxyl group on the ZnO surface, facilitating the formation of chemical bonds and leading to uniform and continuous patterns. Therefore, the duration of citrate modification of ZnO nanoparticles plays an important role in photopatterning. It is recommended that the sodium citrate treatment time should be no less than 36 h to facilitate sufficient carboxyl groups on the ZnO surface (Suppl. Note 4 and Suppl. Fig. 35).

In the photopatterning process, the Zn^{2+} ions are generated upon UV irradiation. Then, ions diffuse from areas of high concentration (irradiated areas) to areas of low concentration (nonirradiated areas). Meanwhile, these ions are consumed by binding to ZnO@Cit. The diffusion of Zn^{2+} ions can result in reduced pattern resolution and pattern distortion during printing. As shown in Suppl. Fig. 11, when the exposure time exceeds 10 s, the small pore features on the butterfly wings gradually disappear, and after 40 s, they completely merge. The extent of these effects depends on the intensity and duration of light exposure. A high light intensity triggers a faster production of Zn^{2+} ions. According to Fick's law of diffusion, a higher concentration gradient drives faster diffusion. Thus, with the same exposure time, higher light intensity causes greater distortion because more Zn^{2+} ions are released, leading to larger local concentration gradients and faster ion diffusion. Additionally, under high light intensity, ZnO particles absorb photon energy and convert it into heat, creating local temperature gradients that induce convection, where the bulk flow of the solution can significantly deteriorate the patterning process, as illustrated in Suppl. Figs. 13b–f, 17. For the same light intensity, longer exposure times allow Zn^{2+} ions to diffuse over a longer period, increasing the diffusion range and the degree of pattern distortion. An effective approach to mitigate the diffusion to nonirradiated areas is to promote the consumption of Zn^{2+} ions (binding to ZnO@Cit), which is achieved by providing sufficiently abundant ligands on ZnO. As mentioned earlier, sufficiently abundant ligands on ZnO can be achieved by a sufficiently long citrate treatment time (over 36 h).

In summary, we demonstrate a rapid, cost-effective, and scalable approach for optical patterning of semiconductor particles by modulating their surface charge through light-induced photochemical reactions. Utilizing ZnO nanoparticles as an example, we have exploited the photocatalytic degradation of surface ligands under UV irradiation to alter the surface charge of ZnO particles, allowing both positive and negative patterning of ZnO nanoparticles onto substrates with tailored electrostatic interactions and high precision. The formation of interparticle chemical bonds in the positive patterning system enables the optical patterning of multilayered ZnO colloidal particles. Our method operates under low light intensities (as low as 6 mW cm^{-2}) and brief exposure times (less than 2 min), significantly reducing energy requirements compared to traditional optical patterning techniques that rely on high-intensity lasers. The developed photodetectors based on patterned ZnO arrays exhibits a high photoconductive gain of up to 10^4, owing to the large surface area and the grating structure that provides a directional carrier path. Our work provides a rapid and effective method for patterning semiconductor nanostructures on substrates, with potential applications in various optoelectronic devices and beyond.

Methods
Materials
Zinc acetate ($Zn(OAc)_2$, 99.5%), zinc nitrate hexahydrate ($Zn(NO_3)_2$·6H_2O, 98%), hexamethylenetetramine (HMTA, 99.5%), sodium citrate tribasic dihydrate ($C_6H_5Na_3O_7$·2H_2O, 98%), sodium hydroxide (NaOH, 99%), diethylene glycol (DEG, 99%), thiourea (99%), 3-mercaptopropionic acid (MPA, 98%), titanium isopropoxide (TTIP, 97%), formic acid (98%), NaCl (99%), ethanol (>99%), acetone (>99%),

poly(dimethyl diallyl ammonium chloride) (PDDA, M_w = 1–20 kg mol^{-1}, 20 wt% aqueous solution), and 3-aminopropyltriethoxysilane (APTES, 98%) were purchased from Shanghai Aladdin (China). Sodium tartrate (TA, 98%), sodium malate (MA, 98%), zinc acetate dihydrate (Zn(CH$_3$COO)$_2$·2H$_2$O, 99.99%), cadmium acetate dihydrate (Cd(CH$_3$COO)$_2$·2H$_2$O, 99.5%), octadecyltrichlorosilane (OTS, C$_{18}$H$_{37}$Cl$_3$Si, 95%), hexane (C$_6$H$_{14}$, 99%), and ammonium hydroxide solution (NH$_3$·H$_2$O, 25–28%) were purchased from Macklin Biochemical. Hydrochloric acid (HCl, 36–38%) and hydrogen peroxide solution (H$_2$O$_2$, 31%) were purchased from Beijing Chemical Reagent. Glass substrates with a thickness of 0.15 μm were purchased from Yangzhou Rongguang Hi-tech Glass Co., Ltd. Conductive indium tin oxide (ITO)-coated glass substrates (<10 Ω sq^{-1}) were obtained from Zhuhai Kaivo Optoelectronic Technology Co., Ltd. Transparent, flexible polyvinyl chloride (PVC) substrates were purchased from Taobao.

Synthesis of ZnO colloidal nanoparticles, ZnO microspheres, and irregularly shaped ZnO nanoparticles

Monodispersed ZnO colloidal nanoparticles with a diameter of 600 nm were prepared through a two-stage reaction[36]. In a typical synthesis, a solution of Zn(OAc)$_2$/DEG was prepared by dissolving 1.83 g of Zn(OAc)$_2$ in 100 mL of DEG. Subsequently, the Zn(OAc)$_2$/DEG solution was heated to 160 °C in an oven for 1 h and cooled to room temperature. The solution was centrifuged at 9030 × g for 10 min to obtain the supernatant, which served as the seed solution for the subsequent growth of ZnO nanoparticles. A second Zn(OAc)$_2$/DEG solution was prepared using the same method described above and heated to 150 °C for 20 min, after which 312 μL of the seed solution was added. The mixture was heated to 170 °C for 2 h. After cooling the solution to room temperature, the product was collected by centrifugation at 7310 × g for 10 min, washed with ethanol and DI water three times, and then dried at 60 °C overnight. Then, the dried product powder was further annealed at 300 °C for 1 h in ambient air to obtain pristine ZnO nanoparticles. The diameter of the ZnO nanoparticles could be tuned by varying the amount of the seeding solution (Suppl. Fig. 1).

The ZnO microspheres were synthesized by thermal decomposition of zinc citrate microspheres[59]. In a typical synthesis, 1.48 g of Zn(NO$_3$)$_2$·6H$_2$O and 0.70 g of HMTA were dissolved in 150 mL of DI water. After stirring for 20 min, the solution was added with 0.56 g of sodium citrate and stirred for an additional 10 min. The solution was heated at 90 °C for 40 min, yielding zinc citrate microspheres, which were collected by centrifugation at 644 × g for 2 min, washed with DI water several times and thermally decomposed at 500 °C for 1 h in air.

The irregular ZnO nanoparticles were prepared using the co-precipitation method. In a typical synthesis, 5.95 g of Zn(NO$_3$)$_2$·6H$_2$O and 1.60 g of NaOH were dissolved in separate beakers with 100 mL DI water. Afterward, the NaOH solution was slowly dropped into the Zn(NO$_3$)$_2$·6H$_2$O solution, and the resulting mixture was stirred for 2 h. Then, white participants were washed with DI water, dried at 60 °C overnight, and thermally treated at 300 °C for 1 h to obtain irregular ZnO nanoparticles.

Surface modification of ZnO particles with citrate, MPA, MA, and TA

To graft citrate onto ZnO, 0.4 g of ZnO nanoparticles, microspheres, or irregular particles, were dispersed in 40 mL of water by ultrasonication. Then, 4 g of sodium citrate was added to the solution, followed by stirring for 48 h. The ZnO@Cit nanoparticles were collected by centrifugation at 1000 × g for 5 min and washed with DI water.

For MPA capping, 0.1 g of ZnO nanoparticles were dispersed in 40 mL of DI water by sonication, followed by the addition of 200 μL of MPA. The pH was adjusted to 9–10 by adding 2 M NaOH. After stirring for 24 h, ZnO@MPA nanoparticles were collected by centrifugation at 1000 × g for 5 min and washed with DI water to remove free MPA ligands in the solution.

To cap MA ligands on the ZnO surface, 0.1 g of ZnO nanoparticles dispersed in 20 mL of DI water by sonication, and then mixed with 20 mL of an aqueous solution containing 2 g of MA. The pH value was adjusted to 9–10 by dropwise adding 2 M NaOH. After 48 h, ZnO@MA nanoparticles were collected by centrifugation 1000 × g for 5 min and washed with DI water.

The preparation of ZnO@TA nanoparticles followed the same procedure as ZnO@MA, with TA used for surface modification instead of MA.

Modification of ZnO@Cit nanoparticles with PDDA

Typically, 900 mg of ZnO@Cit nanoparticles were redispersed in 30 mL of 0.1 M NaCl aqueous solution, followed by the dropwise addition of 200 μL of PDDA aqueous solution under vigorous stirring for 2 h. Afterward, the ZnO@Cit/PDDA particles were collected by centrifugation (1000 × g for 5 min) and washed with DI water three times.

Synthesis of ZnS, ZnS@MPA, and ZnS@MPA/PDDA microparticles

ZnS microspheres were synthesized following a reported method[60]. First, 2.195 g of Zn(CH$_3$COO)$_2$·2H$_2$O was dissolved in 80 mL of DI water, followed by a slow addition of 0.609 g of thiourea. After stirring for 5 min, the mixture was transferred into a 100 mL Teflon-lined autoclave and heated at 140 °C for 8 h. The products were collected, thoroughly washed with DI water, and then dried at 60 °C overnight. The resulting white powder was annealed at 300 °C for 1 h to obtain ZnS microspheres. For MPA modification, 0.1 g of ZnS was dispersed in 40 mL of DI water, followed by the addition of 200 μL of MPA. The pH of the mixture was adjusted to 9–10 using 2 M NaOH. After stirring for 12 h, the MPA-capped ZnS (denoted as ZnS@MPA) was collected by centrifugation (644 × g for 2 min) and washed with DI water. PDDA capping on ZnS@MPA microparticles (ZnS@MPA/PDDA) followed the same procedure as for ZnO@Cit.

Synthesis of CdS, CdS@MPA, and CdS@MPA/PDDA nanoparticles

Pristine CdS nanoparticles of uniform size were prepared using a reported method[61]. In a typical synthesis, 3.2 mmol of Cd(CH$_3$COO)$_2$·2H$_2$O and 16 mmol of thiourea were added to 40 mL of DI water, and the mixture was stirred for 30 min. The mixture was then transferred to a 50 mL Teflon-lined autoclave and heated at 140 °C for 5 h. The product was collected via centrifugation (9030 × g for 10 min), washed with DI water several times, and dried in an oven at 60 °C oven overnight. Finally, the pristine CdS was obtained by thermal annealing the yellow product at 300 °C for 1 h in the air. To graft MPA onto CdS, 0.1 g of CdS was dispersed in 40 mL of DI water. Then, 500 μL of MPA was added, and the pH was adjusted to 8–9 with 2 M NaOH. The solution was heated to 50 °C and stirred for 3 h. Afterward, MPA-capped CdS (denoted as CdS@MPA) was collected via centrifugation (9030 × g for 10 min) and washed several times with DI water. The capping of PDDA on CdS@MPA nanoparticles (CdS@MPA/PDDA) follows the same procedure as that used for ZnO@Cit.

Synthesis of pristine TiO$_2$ and TiO$_2$/PDDA microspheres

The pristine TiO$_2$ microspheres were synthesized using TTIP as a precursor[62]. Briefly, 1.3 mL of TTIP was dissolved in 30 mL of ethanol, and the solution was stirred for 5 min. Next, 0.35 mL of formic acid was added. After stirring for 5 min, the mixture solution was transferred to a Teflon-lined autoclave and heated to 150 °C for 2 h. Then, the product was collected via centrifugation (644 × g for 2 min) and washed with ethanol and water three times. The white powder was obtained by

drying at 60 °C overnight, followed by annealing at 450 °C for 2 h. Surface modification of TiO_2 microspheres with PDDA follows the exact same procedure as that used for ZnO@Cit.

Optical patterning

Both positive and negative patterning of semiconductor particles employed the same experimental setup shown in Fig. 2e. For positive patterning, ZnO@Cit nanoparticles were redispersed in DI water at a concentration of 30 mg mL^{-1}. The obtained suspension was dropped onto cleaned and O_2-plasma-treated glass/ITO/PVC substrates. The UV light generated by a 300 W xenon lamp (CEL-HXF300, CEAU-Light, Beijing) passed through a photomask to form a UV pattern on the substrate. After UV irradiation, the substrates with ZnO@Cit nanoparticles were gently rinsed with DI water to remove unbound ZnO nanoparticles in the nonirradiated region, followed by drying in the air. A typical example of positive patterning of ZnO@Cit nanoparticles is shown in Suppl. Movie 2. Following the same procedure, positive patterning was also achieved for ZnO@Cit microspheres, irregular ZnO@Cit nanoparticles, ZnO@MPA, ZnO@MA, ZnO@TA nanoparticles, CdS@MPA nanoparticles, and ZnS@MPA microparticles.

For negative patterning, a dispersion of ZnO@Cit/PDDA nanoparticles (10 mg mL^{-1}) was dropped onto cleaned O_2-plasma-treated substrates, followed by rinsing the substrates with DI water to leave a monolayer of ZnO. UV irradiation was then applied at a low light intensity of 6 mW cm^{-2}. After rinsing with DI water again, a negative pattern was obtained. A typical example of negative patterning of ZnO@Cit/PDDA nanoparticles is shown in Suppl. Movie 3. The negative patterning of other PDDA-terminated semiconductor particles was conducted using the same procedure but with different light intensities and exposure durations. The particle removal efficiency is defined as follows: particle removal efficiency = $(S_{non\text{-}UV} - S_{UV})/S_{non\text{-}UV}$, where $S_{non\text{-}UV}$ is the area of the particles before UV exposure (at $t = 0$ s), and S_{UV} is the area of the particles remaining in the illuminated region after UV exposure.

Preparation of neutral and positively charged substrates

Neutral glass substrates were obtained by modifying them with OTS[58]. Briefly, 2 mL of OTS was added to 20 mL of hexane. Then, clean slides were immersed in solution (OTS: hexane = 1: 10) and incubated for 17 h. After cleaning with ethanol and DI water, the OTS-treated substrates were dried with nitrogen. Glass substrates with a positively charged surface were prepared by functionalizing the substrate with APTES[63]. Before modification, glass slides were cleaned with acetone, ethanol, and DI water using ultrasonication for 10 min. The slides were then immersed in an ammonia solution (NH_3: H_2O_2: $H_2O = 1$:1:5) for 10 min. After thorough rinsing with DI water, the substrates were immersed in a solution of hydrochloric acid (HCl: H_2O_2: $H_2O = 1$:1:5) for 10 min. After cleaning with DI water, the substrates were immersed in an ethanol solution containing 5 vol% APTES (by volume) for 1 h. Finally, they were rinsed with ethanol and dried at 110 °C for 1 h.

Evaluation of the porosity of positively patterned ZnO films

To evaluate the porosity of the ZnO film produced through the positive patterning, we have printed rectangular-shaped and circular-shaped patterns on the glass substrates (Suppl. Fig. 14). The porosity of each pattern was evaluated through the following formula:

$$Porosity = \frac{V_{pattern} - V_{ZnO}}{V_{pattern}} \tag{2}$$

where $V_{pattern}$ is the volume of the pattern, and V_{ZnO} is the volume of ZnO. Since the size of the ZnO nanoparticles is ≈600 nm, the volume of the ligand can be neglected when estimating the porosity. The $V_{pattern}$

was calculated by the Eq. (3):

$$V_{pattern} = S \times h \tag{3}$$

where S represents the area of the pattern and h is the height of the pattern. According to the cross-sectional SEM images of the rectangular and circular patterns, an average height is obtained. The volume of ZnO could be evaluated through the Eq. (4):

$$V = \frac{m}{\rho} \tag{4}$$

where m is the mass of patterned ZnO and ρ is the density of ZnO ($\rho_{ZnO} = 5.609$ g cm^{-3}). The mass of patterned ZnO on the substrate can be calculated by weighing the substrate before and after ZnO patterning. Before weighing, substrates with patterned ZnO are dried in an oven at 80 °C for 1 h to completely remove moisture. Suppl. Table 2 shows the measured dataset for evaluating the porosity of positively patterned ZnO films. The calculated average porosity is ≈66.82%, indicating that ZnO nanoparticles are loosely packed.

ICP-MS test

Before UV irradiation, the ZnO@Cit colloidal nanoparticles were washed with DI water five times to ensure the complete removal of Zn^{2+} and Na^+ ions from the solution. Then, the ZnO@Cit colloidal particles were redispersed in DI water to obtain a dispersion with a concentration of 30 mg mL^{-1}. Subsequently, 15 mL of the ZnO@Cit particle solution was divided into 15 equal portions and placed in small glass bottles to undergo UV exposure with varying exposure times (5, 10, 15, 20, and 25 s) at two different light intensities (6 and 18 mW cm^{-2}). Afterward, each dispersion was centrifuged for 15 min at 9030 × g, and 100 μL of the supernatant was redispersed in 5 mL of DI water. Quantitative analysis of the Zn^{2+} ions in the dispersions was performed by ICP-MS (Agilent 7700X).

Fabrication of UV detector

Initially, ZnO arrays with a linewidth of 50 μm and a spacing of 180 μm were photopatterned onto a glass substrate. Then, a thin layer of 5 nm Cr/60 nm Au was deposited on the ZnO arrays through an e-beam evaporator (HHV TF500 Box Coaters). The optoelectronic performance of the designed ZnO photodetector under illumination with 365 nm light was characterized using a semiconductor parameter analyzer (4200, Keithley) at room temperature in air (relative humidity of 30%).

Characterization techniques

Digital images of various ZnO patterns were taken using a digital camera (Nikon D7500). Electron microscopy images of the ZnO patterns were obtained using field-emission scanning electron microscopy (SEM, ZEISS Merlin). The diameter of the ZnO nanocrystal clusters was analyzed through ImageJ. High-resolution transmission electron microscopy (HRTEM) images of the ZnO nanoparticles were taken with an FEI Tecnai G2 F30 transmission electron microscope. Zeta potential measurements were conducted with a PALS Zeta Potential Analyzer (Brookhaven Instruments). X-ray photoelectron spectroscopy (XPS) was performed with an X-ray photoelectron spectrometer (Thermo Scientific). Fourier transform infrared (FTIR) spectroscopy was carried out using an infrared spectrophotometer (TJ270-30A, Tianjin, China) with a spectral resolution of 4 cm^{-1}.

Reporting summary

Further information on research design is available in the Nature Portfolio Reporting Summary linked to this article.

Data availability
The data that support the findings of this study are available from the corresponding authors upon request. Source data are provided with this paper.

References
1. Koman, V. B. et al. Colloidal nanoelectronic state machines based on 2D materials for aerosolizable electronics. *Nat. Nanotechnol.* **13**, 819–827 (2018).
2. Liu, A. T. et al. Colloidal robotics. *Nat. Mater.* **22**, 1453–1462 (2023).
3. Zhao, J. et al. Large-area patterning of full-color quantum dot arrays beyond 1000 pixels per inch by selective electrophoretic deposition. *Nat. Commun.* **12**, 4603 (2021).
4. Polat, E. O. et al. Flexible graphene photodetectors for wearable fitness monitoring. *Sci. Adv.* **5**, eaaw7846 (2019).
5. Zhang, P. et al. Integrated 3D printing of flexible electroluminescent devices and soft robots. *Nat. Commun.* **13**, 4775 (2022).
6. Xia, N. et al. Dynamic morphological transformations in soft architected materials via buckling instability encoded heterogeneous magnetization. *Nat. Commun.* **13**, 7514 (2022).
7. Rajput, S. et al. 2D Nanosilicate for additive manufacturing: rheological modifier, sacrificial ink and support bath. *Bioprinting* **25**, e00187 (2022).
8. Su, L. et al. Modularized microrobot with lock-and-detachable modules for targeted cell delivery in bile duct. *Sci. Adv.* **9**, eadj0883 (2023).
9. Maurer, J. H. M. et al. Direct nanoimprinting of a colloidal self-organizing nanowire ink for flexible, transparent electrodes. *Adv. Mater. Technol.* **2**, 1700034 (2017).
10. Doherty, C. M. et al. Combining UV lithography and an imprinting technique for patterning metal-organic frameworks. *Adv. Mater.* **25**, 4701–4705 (2013).
11. Kuang, M. et al. Inkjet printing patterned photonic crystal domes for wide viewing-angle displays by controlling the sliding three phase contact line. *Adv. Opt. Mater* **2**, 34–38 (2014).
12. Zub, K., Hoeppener, S. & Schubert, U. S. Inkjet printing and 3D printing strategies for biosensing, analytical, and diagnostic applications. *Adv. Mater.* **34**, 2105015 (2022).
13. Salaita, K., Wang, Y. & Mirkin, C. A. Applications of dip-pen nanolithography. *Nat. Nanotechnol.* **2**, 145–155 (2007).
14. Chen, X., Lin, L., Li, Z. & Sun, H. B. Light-directed assembly of colloidal matter. *Adv. Funct. Mater.* **32**, 2104649 (2022).
15. Wang, Y., Fedin, I., Zhang, H. & Talapin, D. V. Direct optical lithography of functional inorganic nanomaterials. *Science* **357**, 385–388 (2017).
16. Chen, M. et al. Programmable dynamic shapes with a swarm of light-powered colloidal motors. *Angew. Chem. Int. Ed.* **60**, 16674–16679 (2021).
17. Nan, F. & Yan, Z. Light-driven self-healing of nanoparticle-based metamolecules. *Angew. Chem. Int. Ed.* **58**, 4917–4922 (2019).
18. Urban, A. S., Lutich, A. A., Stefani, F. D. & Feldmann, J. Laser printing single gold nanoparticles. *Nano Lett.* **10**, 4794–4798 (2010).
19. Pauzauskie, P. J. et al. Optical trapping and integration of semiconductor nanowire assemblies in water. *Nat. Mater.* **5**, 97–101 (2006).
20. Lin, L. et al. Opto-thermoelectric nanotweezers. *Nat. Photonics* **12**, 195–201 (2018).
21. Herber, M., Lengle, D., Valandro, S. R., Wehrmeister, M. & Hill, E. H. Bubble printing of $Ti_3C_2T_X$ MXene for patterning conductive and plasmonic nanostructures. *Nano Lett.* **23**, 6308–6314 (2023).
22. Lin, L. et al. Bubble-pen lithography. *Nano Lett.* **16**, 701–708 (2016).
23. Jamshidi, A. et al. NanoPen: dynamic, low-power, and light-actuated patterning of nanoparticles. *Nano Lett.* **9**, 2921–2925 (2009).
24. Zhang, S. et al. Patterned optoelectronic tweezers: a new scheme for selecting, moving, and storing dielectric particles and cells. *Small* **14**, 1803342 (2018).
25. Yang, J. et al. High-resolution patterning of colloidal quantum dots via non-destructive, light-driven ligand crosslinking. *Nat. Commun.* **11**, 2874 (2020).
26. Hahm, D. et al. Direct patterning of colloidal quantum dots with adaptable dual-ligand surface. *Nat. Nanotechnol.* **17**, 952–958 (2022).
27. Liu, D. et al. Direct optical patterning of perovskite nanocrystals with ligand cross-linkers. *Sci. Adv.* **8**, eabm8433 (2022).
28. Boles, M. A., Ling, D., Hyeon, T. & Talapin, D. V. The surface science of nanocrystals. *Nat. Mater.* **15**, 141–153 (2016).
29. Cho, H. et al. Direct optical patterning of quantum dot light-emitting diodes via in situ ligand exchange. *Adv. Mater.* **32**, 2003805 (2020).
30. Pan, J.-A., Ondry, J. C. & Talapin, D. V. Direct Optical Lithography of $CsPbX_3$ nanocrystals via photoinduced ligand cleavage with post-patterning chemical modification and electronic coupling. *Nano Lett.* **21**, 7609–7616 (2021).
31. Ko, J., Ma, K., Joung, J. F., Park, S. & Bang, J. Ligand-assisted direct photolithography of perovskite nanocrystals encapsulated with multifunctional polymer ligands for stable, full-colored, high-resolution displays. *Nano Lett.* **21**, 2288–2295 (2021).
32. Lee, K. M., Lai, C. W., Ngai, K. S. & Juan, J. C. Recent developments of zinc oxide based photocatalyst in water treatment technology: a review. *Water Res.* **88**, 428–448 (2016).
33. Joshi, P., Ansari, Z. A., Singh, S. P. & Shanker, V. Synthesis and characterization of highly fluorescent water dispersible ZnO quantum dots. *Adv. Sci. Lett.* **2**, 360–363 (2009).
34. Quici, N., Morgada, M. E., Gettar, R. T., Bolte, M. & Litter, M. I. Photocatalytic degradation of citric acid under different conditions: TiO_2 heterogeneous photocatalysis against homogeneous photolytic processes promoted by Fe(III) and H_2O_2. *Appl. Catal. B* **71**, 117–124 (2007).
35. Chevalier-César, C. et al. Direct holographic patterning of ZnO. *Adv. Funct. Mater.* **26**, 1787–1792 (2016).
36. Seelig, E. W., Tang, B., Yamilov, A., Cao, H. & Chang, R. P. H. Self-assembled 3D photonic crystals from ZnO colloidal spheres. *Mater. Chem. Phys.* **80**, 257–263 (2003).
37. Hu, X., Gong, J., Zhang, L. & Yu, J. C. Continuous size tuning of monodisperse ZnO colloidal nanocrystal clusters by a microwave-polyol process and their application for humidity sensing. *Adv. Mater.* **20**, 4845–4850 (2008).
38. Fanizza, E. et al. UV-light-driven immobilization of surface-functionalized oxide nanocrystals onto silicon. *Adv. Funct. Mater.* **17**, 201–211 (2007).
39. Walker, D., Singh, D. P. & Fischer, P. Capture of 2D microparticle arrays via a UV-triggered thiol-yne "click" reaction. *Adv. Mater.* **28**, 9846–9850 (2016).
40. Liu, S. F. et al. 3D nanoprinting of semiconductor quantum dots by photoexcitation-induced chemical bonding. *Science* **377**, 1112–1116 (2022).
41. Lin, L. et al. Light-directed reversible assembly of plasmonic nanoparticles using plasmon-enhanced thermophoresis. *ACS Nano* **10**, 9659–9668 (2016).
42. Wang, H. et al. Light-driven magnetic encoding for hybrid magnetic micromachines. *Nano Lett.* **21**, 1628–1635 (2021).
43. Zhang, S. et al. Integrated assembly and photopreservation of topographical micropatterns. *Small* **17**, 2103702 (2021).
44. Gu, Y. & Li, D. The ζ-potential of glass surface in contact with aqueous solutions. *J. Colloid Interface Sci.* **226**, 328–339 (2000).
45. Scaeteanu, G. V., Maxim, C., Badea, M. & Olar, R. Zinc(II) carboxylate coordination polymers with versatile applications. *Molecules* **28**, 1132 (2023).

46. Meng, Y. et al. A phase change supramolecular assembly with a rapid self-healing behavior via thermally actuated reversible associations. *Chem. Eng. J.* **453**, 139967 (2023).

47. Noei, H. et al. The identification of hydroxyl groups on ZnO nanoparticles by infrared spectroscopy. *Phys. Chem. Chem. Phys.* **10**, 7092–7097 (2008).

48. Yin, S. J., Zheng, G. C., Yi, X., Lv, G. P. & Yang, F. Q. A metal-organic framework@hydrogen-bond framework as a matrix for MALDI-TOF-MS analysis of small molecules. *Chem. Commun.* **58**, 6701–6704 (2022).

49. Deacon, G. B. & Phillips, R. J. Relationships between the carbon-oxygen stretching frequencies of carboxylato complexes and the type of carboxylate coordination. *Coord. Chem. Rev.* **33**, 227–250 (1980).

50. Hirose, S., Kobashigawa, K., Izuta, Y. & Hatakeyama, H. Thermal degradation of polyurethanes containing lignin studied by TG-FTIR. *Polym. Int.* **47**, 247–256 (1998).

51. Priyadarshi, R., Kumar, B. & Rhim, J.-W. Green and facile synthesis of carboxymethylcellulose/ZnO nanocomposite hydrogels cross-linked with Zn^{2+} ions. *Int. J. Biol. Macromol.* **162**, 229–235 (2020).

52. Sun, Y. et al. Calligraphy/painting based on a bioinspired light-driven micromotor with concentration-dependent motion direction reversal and dynamic swarming behavior. *ACS Appl. Mater. Interfaces* **11**, 40533–40542 (2019).

53. Hu, Y., Liu, W. & Sun, Y. Multiwavelength phototactic micromotor with controllable swarming motion for "chemistry-on-the-fly". *ACS Appl. Mater. Interfaces* **12**, 41495–41505 (2020).

54. Zhao, L. et al. One-step solvothermal synthesis of a carbon@TiO_2 dyade structure effectively promoting visible-light photocatalysis. *Adv. Mater.* **22**, 3317–3321 (2010).

55. Li, H. et al. Controllable heterogeneous nucleation for patterning high-quality vertical and horizontal ZnO microstructures toward photodetectors. *Small* **16**, 2004136 (2020).

56. Nasiri, N., Bo, R., Wang, F., Fu, L. & Tricoli, A. Ultraporous electron-depleted ZnO nanoparticle networks for highly sensitive portable visible-blind UV photodetectors. *Adv. Mater.* **27**, 4336–4343 (2015).

57. Park, C., Lee, J., So, H. M. & Chang, W. S. An ultrafast response grating structural ZnO photodetector with back-to-back Schottky barriers produced by hydrothermal growth. *J. Mater. Chem. C* **3**, 2737–2743 (2015).

58. Sharma, S. & Conrad, J. C. Attachment from flow of escherichia coli bacteria onto silanized glass substrates. *Langmuir* **30**, 11147–11155 (2014).

59. Xie, Q., Li, J., Tian, Q. & Shi, R. Template-free synthesis of zinc citrate yolk-shell microspheres and their transformation to ZnO yolk-shell nanospheres. *J. Mater. Chem.* **22**, 13541–13547 (2012).

60. Chen, Y., Ma, Q., Jia, H. & Wang, Y. Hydrothermal synthesis of ZnS microspheres with highly effective photocatalytic and antibacterial properties. *J. Mater. Sci. Mater. Electron.* **27**, 10237–10243 (2016).

61. Wang, Z. et al. Self-assembly of three-dimensional CdS nanosphere/graphene networks for efficient photocatalytic hydrogen evolution. *J. Energy Chem.* **31**, 34–38 (2019).

62. He, K., Zhao, G. & Han, G. Template-free synthesis of TiO_2 microspheres with tunable particle size via a non-aqueous sol-gel process. *CrystEngComm* **16**, 7881–7884 (2014).

63. Qin, M. et al. Two methods for glass surface modification and their application in protein immobilization. *Colloids Surf. B: Biointerfaces* **60**, 243–249 (2007).

Acknowledgements

Author contributions

C.H. and X.H. conceived the original idea and designed the experiment. H.G., L.G., Z.Y., and C.H. supervised the project, and X.H. and X.F. performed the experiments. X.H., H.G., Z.Y., and C.H. wrote the paper. Y.M. and H.J. performed the SEM tests, and Y.C. and H.X. analyzed the data. Y.Z. fabricated the photodetector device. M.Y. and H.X. performed the FTIR and XRD analysis. All authors discussed the results and commented on the manuscript.

Competing interests

The authors declare no competing interests.

Additional information

Supplementary information The online version contains supplementary material available at https://doi.org/10.1038/s41467-024-53926-7.

Correspondence and requests for materials should be addressed to Zhan Yang or Chengzhi Hu.

Peer review information *Nature Communications* thanks Shuailong Zhang and the other, anonymous, reviewers for their contribution to the peer review of this work. A peer review file is available.

Reprints and permissions information is available at http://www.nature.com/reprints

Publisher's note Springer Nature remains neutral with regard to jurisdictional claims in published maps and institutional affiliations.